Global direct and adjoint modes of a hypersonic flow over a cone

By T. J. Flint AND M. J. P Hack

1. Motivation and objectives

In high-speed flows boundary-layer transition has consequences not only for drag but for heat transfer too. This makes it an important flow feature to predict in order to design efficient vehicles (Leyva 2017). So-called natural transition, which may occur in quiet flow conditions such as that found in the upper atmosphere, has long been studied and is preceded by the amplification of linear instabilities in the boundary layer up until their amplitude becomes large enough that non-linearity facilitates breakdown to turbulence (Fedorov 2011). The study of the linear regime preceding transition can provide key insight into the transition process (see, e.g., Unnikrishnan & Gaitonde (2020)) while the linear framework makes the problem significantly more tractable than studying the full non-linear problem. Traditionally, linear analysis has leveraged the assumption that the boundary layer is locally parallel in order to simplify the analysis (see, e.g., Mack (1975); Malik (1990)). One of the difficulties with using local linear analysis to predict transition is that the initial amplitude of the amplifying disturbance within the boundary layer is unknown and depends on the free stream perturbation field and its interaction with the boundary layer, the so-called receptivity process (see, e.g., Morkovin (1969); Reshotko (1976)). In fact, non-parallel regions of the flow field, such as leading edges, have long been known to be important to the receptivity process (see, e.g., Goldstein & Hultgren (1989)). In addition to leading-edge effects, the presence of shocks are known to amplify incoming disturbances (Ribner 1953), making them relevant to the receptivity process also.

With widespread access to high-performance computing resources, more sophisticated analyses are possible. One such analysis, which we pursue here, is global stability (Theofilis 2011) and adjoint receptivity analysis (Luchini & Bottaro 2014; Meneghello *et al.* 2015; Gianetti & Luchini 2007). In the context of a linear analysis, the global approach removes all *a-priori* assumptions about the base flow apart from the validity of the underlying governing equations. Non-parallel flow features and the presence of shocks are naturally included in the analysis. In contrast to local analyses, in which one may perform many independent analyses at different locations in the flow field, the global analysis unifies modes at all locations within the domain and provides a complete picture of the temporal response of the flow field including non-parallel effects and complex interactions between various locations in the domain. The adjoint receptivity analysis can directly compute the receptivity of these global modes to the free stream disturbance field, providing a complete picture of the linear response which is not possible with the local analysis (Luchini & Bottaro 2014).

A geometry relevant to many high-speed aerodynamic vehicles is a blunt-nose cone. Here we focus on a right circular cone with a spherically blunted nose (see, e.g., Stetson *et al.* (1984)). While local analysis has provided important information about the nature of amplifying modes within the boundary layer, missing from the literature is a rigorous

receptivity analysis of this geometry. The receptivity problem for this case has been investigated by others using direct numerical simulation (DNS) (Zhong & Ma 2006) and input-output (resolvent) analysis (Nichols & Candler 2019), though both of these methods have limitations. Direct numerical simulation is costly and the user must prescribe a particular free stream disturbance to study. Input-output analysis requires a parametric study over frequency space to find the most relevant disturbances. The global analysis overcomes the aforementioned limitations by directly identifying the most efficient free stream forcing field through the adjoint eigenmodes, while important frequencies are simply given by the eigenvalues of the direct linearized system.

This work directly identifies the spatial structure of modes that may lead to transition through the direct eigenvalue problem. The receptivity of these direct modes to disturbances in the free stream are rigorously identified as the corresponding adjoint eigenmodes, thus completing the picture of the linear processes that precede natural transition on a blunt cone at high speed. In the case of the blunt cone, non-modal growth may become important to transition as the nose bluntness is increased (Paredes *et al.* 2020) and global analysis can be used to study this problem also, though this is not the focus of the present report.

2. Methodology

For details of the governing equations and the numerical framework the reader is referred to Flint & Hack (2018), with the key details mentioned briefly here. The flow of a compressible, perfect gas, in chemical and thermal equilibrium, in the continuum regime, and with a temperature-dependent viscosity is considered. The flow field is decomposed into a base state and a linear disturbance,

$$\mathbf{q} = \bar{\mathbf{q}} + \mathbf{q}', \tag{2.1}$$

where $\mathbf{q} = [\rho, \rho u, \rho v, \rho w, E]^{\mathsf{T}}$ is the flow state vector made up of density, momentum in the x, y, and z directions, and total energy. The steady base state and linear disturbance components are denoted $\bar{\mathbf{q}}$ and $\mathbf{q}'$, respectively. The Navier-Stokes equations are time advanced to a steady-state solution to provide a base state for the linearized equations. Because the flow considered is absolutely stable (Huerre & Monkewitz 1990) no special treatment is required in order to converge to a steady solution. The linearized compressible Navier-Stokes equations can then be formulated as

$$\frac{\partial \mathbf{q}'}{\partial t} + \mathsf{L}\mathbf{q}' = 0, \tag{2.2}$$

where L is the linearized Navier-Stokes operator, and t is time. Since L is independent of t, we introduce a normal-mode ansatz of the form

$$\mathbf{q}'(\boldsymbol{x}, t) = \hat{\mathbf{q}}(\boldsymbol{x}) \exp(-\mathrm{i}\omega t), \tag{2.3}$$

where ω is a complex frequency. Substituting this ansatz into the linear equations, (2.2), yields the global, direct, eigenvalue problem,

$$\mathsf{L}\hat{\mathbf{q}} = \lambda \hat{\mathbf{q}}, \tag{2.4}$$

$$\lambda = -\mathrm{i}\omega. \tag{2.5}$$

The corresponding adjoint eigenvalue problem is defined as

$$\mathsf{L}^{\dagger}\hat{\mathbf{q}}^{\dagger} = \lambda^{\dagger}\hat{\mathbf{q}}^{\dagger}, \tag{2.6}$$

Property	Value
Cone half angle, θ	7°
Wall temperature, T_w	T_∞
Free stream Mach number, Ma_∞	6
Reynolds number based on tip radius, Re_R	12000
Ratio of specific heats, γ	1.4
Prandtl number, Pr	0.71
Viscosity temperature exponent, α	0.7

TABLE 1. Parameters used for the cone simulation.

where the superscript † denotes the adjoint of the corresponding direct counterpart.

Here, the direct and adjoint operators, L and $\mathsf{L}^\dagger$, are formed by discretizing the continuous direct and adjoint linearized Navier-Stokes equations. The equations are discretized on a structured axisymmetric curvilinear grid using fourth-order central differences. The pole at the axis of the axisymmetric coordinate system is handled by smoothly differentiating through the pole and avoiding the singular point (Mohseni & Colonius 2000). For the base state calculation, shocks are captured using artificial bulk viscosity (Mani *et al.* 2009; Kawai & Lele 2008; Kawai *et al.* 2010). Time advancement, used when solving the eigenvalue problem (see Section 2.1), uses a fourth-order Runge-Kutta scheme. Stabilization during time advancement is achieved by applying a weak low-pass compact filter (Lele 1992); such stabilization has been used and validated in many other studies (see Nagarajan (2004)).

To understand the meaning of the adjoint eigenmodes, consider that the effect of time harmonic forcing on the perturbation field can be accounted for by introducing a source term into the governing equations

$$\frac{\partial \mathbf{q}'}{\partial t} + \mathsf{L}\mathbf{q}' = \mathbf{f}'. \tag{2.7}$$

For the spatial stability problem, Hill (1995) showed that the adjoint eigenfunction, $\hat{\mathbf{q}}^\dagger$, acts as a weight on a time-harmonic forcing field, $\hat{\mathbf{f}}$. The streamwise growth in the amplitude of the perturbation eigenfunction, $\hat{\mathbf{q}}$, is obtained as the integral of the projection of the forcing field onto the corresponding adjoint eigenfunction. Hence, for the forcing to most effectively influence the amplitude of the disturbance field, it should be applied in regions where the magnitude of the adjoint eigenfunction is large, which introduces a mathematically rigorous definition of disturbance receptivity. An extension of the adjoint-based receptivity analysis to the temporal problem considered within this work was introduced by Gianetti & Luchini (2007).

2.1. *Solving the eigenvalue problem*

A spectral transformation is used to accelerate the convergence of eigenvalues of interest. We target the most unstable modes which will have the most positive $\mathcal{I}(\omega)$, or equivalently the most positive $\mathcal{R}(\lambda)$. The eigenvalue spectrum is transformed using an approximate exponential transform (see, e.g., Eriksson & Rizzi (1985); Meerbergen & Roose (1996); Theofilis (2011)),

$$\mathrm{e}^{\mathsf{L}\Delta t}\hat{\mathbf{q}} = \mathrm{e}^{\lambda\Delta t}\hat{\mathbf{q}}. \tag{2.8}$$

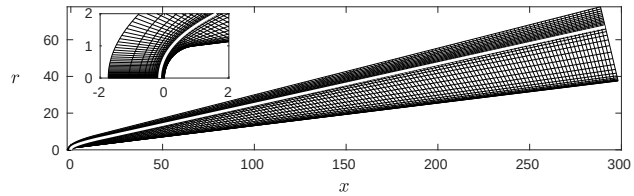

FIGURE 1. Computational mesh used for the blunt cone simulation with the cylindrical coordinate system shown. The mesh is axisymmetric about the x axis. Note that only every 16th row and column are shown to aid visualization. The approximate shock location is indicated with a thick white line.

The transformed system, $\mathrm{e}^{\mathsf{L}\Delta t}\hat{\mathbf{q}}$, is approximated by time advancing the state, $\hat{\mathbf{q}}$, for a time horizon Δt using a fourth-order Runge-Kutta scheme. The user-defined parameter, Δt, can be chosen to provide a trade-off between improved eigenvalue convergence due to improved eigenvalue separation and the computational cost incurred to time march for Δt. By transforming the system, the transformed eigenvalues, $\phi = \mathrm{e}^{\lambda\Delta t}$, have the largest magnitude for the most temporally unstable modes.

We find a subset of the largest magnitude eigenvalues using the implicitly restarted Arnoldi method implemented in PARPACK (Maschhoff & Sorensen 1996). This is a matrix-free method that is well suited for the large eigenvalue problems that are considered in global stability analysis and has been used in a number of other similar studies (see, e.g., Mack & Schmid (2011); Nichols & Lele (2011); Mack & Schmid (2010)).

3. Flow conditions

The case considered in this report is Mach 6 flow over a spherically blunted cone. The parameters used in the cone simulation are presented in Table 1. The cone has an isothermal wall with a temperature equal to that of the free stream temperature, T_∞, making it a highly cooled wall.

The axisymmetric computational mesh consists of 512 nodes in the cone-normal direction and 4096 nodes in the cone-tangential direction, the structure of which is shown in Figure 1. This grid size results in a sparse eigenvalue problem with 10,485,760 degrees of freedom. The mesh is refined toward the cone surface, the axis, and at the shock. The grid lines are tangential to the shock at all locations along the shock. The free stream boundaries are imposed with a sponge layer for both the base flow and the eigenvalue calculations, and the wall is a no-slip wall. The magnitude of the eigenvectors are prescribed to be zero at the free stream boundaries.

Contours of Mach number for the computed base flow are shown in Figure 2 with the flow coming from left to right. The shock is included within the computational domain and the stand-off distance of the bow shock agrees well with the model by Van Dyke (1958) for a parabolic shock over blunt bodies. The shock angle asymptotically approaches $\sim$11.97°, as predicted by Maccoll (1937) for inviscid flow over a sharp cone. An indication of the edge of the boundary layer in the downstream half of the domain is given by the contour of 99% of the Mach number at the surface as predicted by inviscid sharp cone theory (Maccoll 1937).

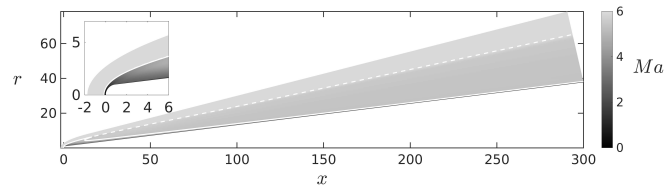

FIGURE 2. Base flow Mach number contours with insert showing the region near the blunt nose in more detail. The dashed line indicates the shock position and the solid line indicates the contour of 99% of the Mach number at the surface as predicted for an inviscid sharp cone (Maccoll 1937).

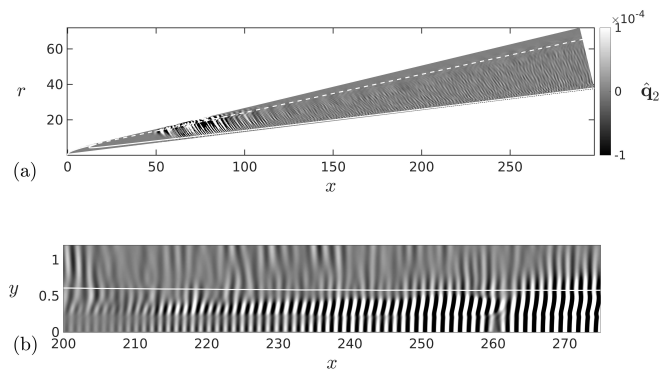

FIGURE 3. A direct mode with an azimuthal wavenumber of 0, the streamwise momentum component of the mode, $\hat{\mathbf{q}}_2$, is shown. The full global mode, (a), and a zoom of the boundary layer in the region $200 < x < 275$, (b).

4. Results

4.1. *Direct mode*

One of the direct modes with an azimuthal wavenumber of 0 is shown in Figure 3. As a consequence of the large domain size, the small cell size near the stagnation point, and the resulting time-step restriction, converging the modes using the exponential transform as described in Section 2 becomes difficult due to clustering of the eigenvalues. As such, this mode is not fully converged, though it does exhibit some physical features which may become more pronounced as it is further converged. Most of the domain is relatively quiet except for a large region between $x = 50$ and $x = 100$, and within the boundary layer beyond $x \approx 210$. While the upstream region may be an artifact at this stage of the convergence, the part of the global mode within the boundary layer resembles physical second-mode waves. The boundary layer in the region of growth is shown in detail in Figure 3(b) in which it is clear that the mode is trapped within the boundary layer and exhibits streamwise amplification.

Profiles through the boundary layer at $x \approx 240$ are shown in Figure 4. The structure of the mode is now more obvious: the two velocity components (Figure 4(a,b)) show a large wide peak near the wall followed by a smaller peak further away from the wall. The pressure component (Figure 4(c)) has maximum amplitude at the wall, and the temperature component (Figure 4(d)) has two peaks in amplitude within the boundary layer. The structure of this mode resembles that of Mack's second-mode obtained with

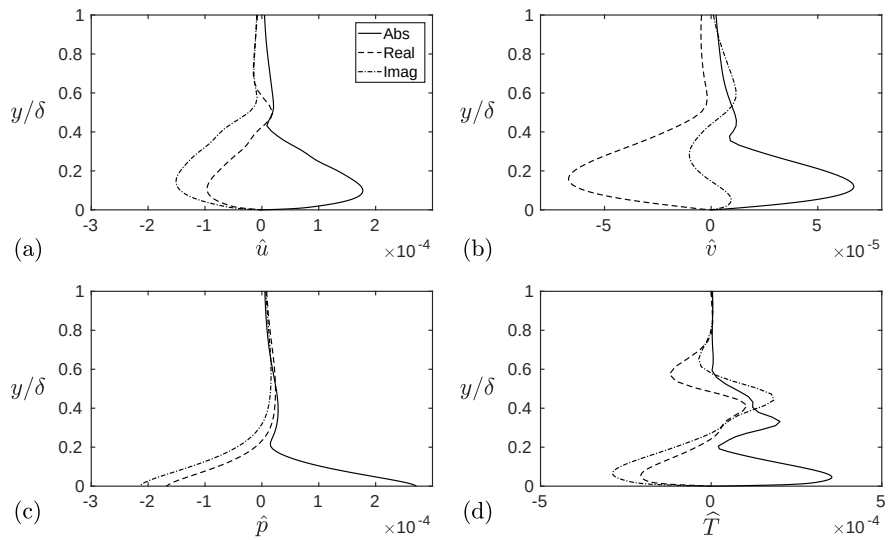

FIGURE 4. Profiles through the boundary layer of the direct mode at a location of $x \approx 240$. The wall-normal coordinate is normalized by the boundary layer thickness, δ.

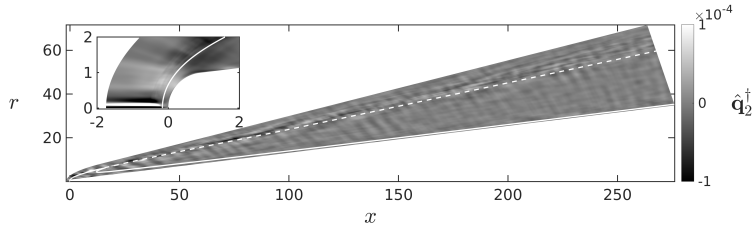

FIGURE 5. An adjoint mode with azimuthal wavenumber of 0 with an insert showing the nose region in detail.

a local analysis of a hypersonic boundary layer (Zhong & Ma 2006), though here this structure is embedded within the global mode. In contrast to the local analysis, the global mode will allow us to directly see how this wave packet interacts with the shock, the blunt nose of the cone, and how it evolves in the streamwise direction. Along with the corresponding adjoint mode (discussed in Section 4.2), a complete picture of how the mode is formed and its receptivity to disturbances in the flow field can be constructed.

4.2. *Adjoint mode*

The adjoint mode provides a spatial map of the receptivity of the corresponding direct mode to momentum forcing (Gianetti & Luchini 2007). An adjoint mode is shown in Figure 5. The eigenfunction shows high amplitude in the region directly upstream of the shock near the stagnation point, indicating that this flow field is most receptive to forcing here. The adjoint mode decreases in amplitude through the shock, which may be reasoned by the fact that disturbances introduced before the shock will get amplified as they pass through, whereas this will not be the case if introduced downstream (Ribner 1953).

5. Conclusions

Global modes for a blunt cone at Mach 6 have been computed. The global analysis gives a complete picture of the structure of the mode, how it is excited, and how it evolves which is not possible with the traditional local analysis. While the modes presented are preliminary owing to incomplete convergence, they exhibit physical features and offer some insight into the receptivity process for this flow field. The direct mode captures wave-like structures limited to the boundary layer in the downstream portion of the cone which amplifies in the streamwise direction. This mode resembles physical modes that have been observed in other compressible boundary layers, though here it is part of an all-encompassing global mode. The receptivity of this mode is identified by the corresponding adjoint mode, which indicates the highest receptivity is directly upstream of the bow shock near the stagnation point.

Acknowledgments

This investigation was funded by the Office of Naval Research under Grant #N00014-17-1-2341 and the Franklin P. and Caroline M. Johnson Fellowship.

REFERENCES

Eriksson, L. E. & Rizzi, A. 1985 Computer-aided analysis of the convergence to steady state of discrete approximations to the Euler equations. *J. Comput. Phys.* **57**, 90–128.

Fedorov, A. 2011 Transition and stability of high-speed boundary layers. *Annu. Rev. Fluid Mech.* **43**, 79–95.

Flint, T. & Hack, M. J. P. 2018 A computational framework for stability analysis of high-speed flows in complex geometries. *Annual Research Briefs*, Center for Turbulence Research, Stanford University, pp. 221–235.

Gianetti, F. & Luchini, P. 2007 Structural sensitivity of the first instability of the cylinder wake. *J. Fluid Mech.* **581**, 167–197.

Goldstein, M. E. & Hultgren, L. S. 1989 Boundary-layer receptivity to long-wave free-stream disturbances. *Annu. Rev. Fluid Mech.* **21**, 137-166.

Hill, D. C. 1995 Adjoint systems and their role in the receptivity problem for boundary layers. *J. Fluid Mech.* **292**, 183–204.

Huerre, P. & Monkewitz, P. A. 1990 Instabilities in spatially developing flows. *Annu. Rev. Fluid Mech.* **22**, 473–537.

Kawai, S. & Lele, S. K. 2008 Localized artificial diffusivity scheme for discontinuity capturing on curvilinear meshes. *J. Comput. Phys.* **227**, 9498–9526.

Kawai, S., Shankar, S. K. & Lele, S. K. 2010 Assessment of localized artificial diffusivity scheme for large-eddy simulation of compressible turbulent flows. *J. Comput. Phys.* **229**, 1739–1762.

Lele, S. K. 1992 Compact finite difference schemes with spectral-like resolution. *J. Comput. Phys.* **103**, 16–42.

Leyva, I. A. 2017 The relentless pursuit of hypersonic flight. *Phys. Today* **70**, 30–36.

Luchini, P. & Bottaro, A. 2014 Adjoint equations in stability analysis. *Annu. Rev. Fluid Mech.* **46**, 493–517.

Maccoll, J. W. 1937 The conical shock wave formed by a cone moving at a high speed. *Proc. R. Soc. Lond. A. Math. Phys. Sci.* **159**, 459–472.

Mack, C. J. & Schmid, P. J. 2010 A preconditioned Krylov technique for global

hydrodynamic stability analysis of large-scale compressible flows. *J. Comput. Phys.* **229**, 541–560.

Mack, C. J. & Schmid, P. J. 2011 Global stability of swept flow around a parabolic body: features of the global spectrum. *J. Fluid Mech.* **669**, 375–396.

Mack, L. M. 1975 Linear stability theory and the problem of supersonic boundary-layer transition. *AIAA J.* **13**, 278–289.

Malik, M. R. 1990 Numerical methods for hypersonic boundary layer stability. *J. Comput. Phys.* **86**, 376–413.

Mani, A., Larsson, J. & Moin, P. 2009 Suitability of artificial bulk viscosity for large-eddy simulation of turbulent flows with shocks. *J. Comput. Phys.* **228**, 7368–7374.

Maschhoff, K. J. & Sorensen, D. C. 1996 P_ARPACK: An efficient portable large scale eigenvalue package for distributed memory parallel architectures. In *Applied Parallel Computing Industrial Computation and Optimization. Lecture Notes in Computer Science* (ed. J. Waśniewski, J. Dongarra, K. Madsen & D. Olesen), vol. 1184. Springer.

Meerbergen, K. & Roose, D. 1996 Matrix transformations for computing rightmost eigenvalues of large sparse non-symmetric eigenvalue problems. *IMA J. Numer. Anal.* **16**, 297–346.

Meneghello, G., Schmid, P. J. & Huerre, P. 2015 Receptivity and sensitivity of the leading-edge boundary layer of a swept wing. *J. Fluid Mech.* **775**, R1.

Mohseni, K. & Colonius, T. 2000 Numerical treatment of polar coordinate singularities. *J. Comput. Phys.* **157**, 787–795.

Morkovin, M. V. 1969 Critical evaluation of transition from laminar to turbulent shear layers with emphasis on hypersonically travelling bodies. *Air Force Flight Dyn. Lab. Technical report AFFDL-TR-68-149*.

Nagarajan, S. 2004 Leading edge effects in bypass transition. PhD thesis, Stanford University.

Nichols, J. W. & Candler, G. V. 2019 Input-output analysis of complex hypersonic boundary layers. *AIAA Paper 2019-1383*.

Nichols, J. W. & Lele, S. K. 2011 Global modes and transient response of a cold supersonic jet. *J. Fluid Mech.* **669**, 225–241.

Paredes, P., Choudhari, M. M. & Li, F. 2020 Mechanism for frustum transition over blunt cones at hypersonic speeds. *J. Fluid Mech.* **894**, A22.

Reshotko, E. 1976 Boundary-layer stability and transition. *Annu. Rev. Fluid Mech.* **8**, 311–349.

Ribner, H. S. 1953 Convection of a pattern of vorticity through a shock wave. *NACA Rep. 1164* .

Stetson, K. F., Thompson, E. R., Donaldson, J. C. & Siler, L. G. 1984 Laminar boundary layer stability experiments on a cone at Mach 8, part II: blunt cone. In *AIAA Paper 84-0006*.

Theofilis, V. 2011 Global linear instability. *Annu. Rev. Fluid Mech.* **43**, 319–352.

Unnikrishnan, S. & Gaitonde, D. 2020 Linear, nonlinear and transitional regimes of second-mode instability. *J. Fluid Mech.* **905**, A25.

Van Dyke, M. D. 1958 A model of supersonic flow past blunt axisymmetric bodies, with application to Chester's solution. *J. Fluid Mech.* **3**, 515–522.

Zhong, X. & Ma, Y. 2006 Boundary-layer receptivity of Mach 7.99 flow over a blunt cone to free-stream acoustic waves. *J. Fluid Mech.* **556**, 55–103.